

The strain-induced transitions of the piezoelectric, pyroelectric and electrocaloric properties of the CuInP_2S_6 films

Anna N. Morozovska¹, Eugene A. Eliseev², Lesya P. Yurchenko², Valentin V. Laguta², Yongtao Liu⁴, Sergei V. Kalinin^{5*}, Andrei L Kholkin^{6†}, and Yulian M. Vysochanskii^{7‡}

¹ Institute of Physics, National Academy of Sciences of Ukraine,
46, Prospekt Nauky, 03028 Kyiv, Ukraine,

² Institute for Problems of Materials Science, National Academy of Sciences of Ukraine,
3, Krjijanovskogo, 03142 Kyiv, Ukraine,

⁵ Center for Nanophase Materials Sciences, Oak Ridge National Laboratory,
Oak Ridge, TN 37922, United States,

⁵ Department of Materials Science and Engineering, University of Tennessee,
Knoxville, TN, 37996, United States,

⁶ Department of Physics & CICECO – Aveiro Institute of Materials, Campus
Universitario de Santiago, 3810-193 Aveiro, Portugal,

⁷ Institute of Solid-State Physics and Chemistry, Uzhhorod University,
88000 Uzhhorod, Ukraine.

Abstract

The low-dimensional ferroelectrics, ferrielectrics and antiferroelectrics are of urgent scientific interest due to their unusual polar, piezoelectric, electrocaloric and pyroelectric properties. The strain engineering and strain control of the ferroelectric properties of layered 2D Van der Waals materials, such as $\text{CuInP}_2(\text{S},\text{Se})_6$ monolayers, thin films and nanoflakes, are of fundamental interest and especially promising for their advanced applications in nanoscale nonvolatile memories, energy conversion and storage, nano-coolers and sensors. Here, we study the polar, piezoelectric, electrocaloric and pyroelectric properties of thin strained films of a ferrielectric CuInP_2S_6 covered by semiconducting electrodes and reveal an unusually strong effect of a mismatch strain on these properties. In particular, the sign of the mismatch strain and its

* Corresponding author: sergei2@utk.edu

† Corresponding author: kholkin@ua.pt

‡ Corresponding author: vysochanskii@gmail.com

magnitude determine the complicated behavior of piezoelectric, electrocaloric and pyroelectric responses. The strain effect on these properties is opposite, i.e., “anomalous”, in comparison with many other ferroelectric films, for which the out-of-plane remanent polarization, piezoelectric, electrocaloric and pyroelectric responses increase strongly for tensile strains and decrease or vanish for compressive strains.

I. INTRODUCTION

The piezoelectric, pyroelectric and electrocaloric effects are inherent to ferroelectrics, being a consequence of their spontaneous polarization dependence on strain and temperature, which becomes especially strong in the vicinity of the paraelectric - ferroelectric phase transition. These properties determine the indispensable value of ferroelectrics for modern actuators, pyroelectric sensors, electromechanical and electrocaloric energy converters [1, 2].

The low-dimensional ferroelectrics, ferrielectrics and antiferroelectrics are of urgent scientific interest due to their unusual polar, piezoelectric, electrocaloric and pyroelectric properties [3, 4]. The strain engineering and strain control of the ferroelectric properties of layered 2D Van der Waals (**V-d-W**) materials, such as $\text{CuInP}_2(\text{S,Se})_6$ monolayers, thin films and nanoflakes, are of fundamental interest and especially promising for their advanced applications in nanoscale nonvolatile memories, energy conversion and storage, nano-coolers and sensors [5].

One of the most important feature, which determine the strain-polarization coupling in ferrielectrics $\text{CuInP}_2(\text{S,Se})_6$ [6, 7], is the existence of more than two potential wells [8], which are responsible for strain-tunable multiple polar states [9]. Due to the multiple potential wells, which height and position are temperature- and strain-dependent, the energy profiles of a uniaxial ferrielectric $\text{CuInP}_2(\text{S,Se})_6$ can flatten in the vicinity of the nonzero polarization states. The flatten energy profiles give rise to the unusual polar and dielectric properties associated with the strain-polarization coupling in the vicinity of the states [10, 11, 12].

The spontaneous polarization of crystalline CuInP_2S_6 (**CIPS**) is directed normally to its structural layers being a result of antiparallel shifts of the Cu^+ and In^{3+} cations from the middle of the layers [13, 14]. The strain effect on the polarization reversal in CIPS is opposite, i.e., “anomalous”, in comparison with many other ferroelectric films, for which the out-of-plane remanent polarization and coercive field increase strongly for tensile strains, and decrease or vanish for compressive strains [9 - 12].

Using the Landau-Ginzburg-Devonshire (**LGD**) approach here we study the size- and strain-induced changes of the spontaneous polarization, piezoelectric, pyroelectric and electrocaloric properties of thin strained CIPS films covered by semiconducting electrodes. The

original part of this work contains the physical description of the problem (**Section II**), analysis the strain-induced transitions of the piezoelectric, electrocaloric and pyroelectric properties of the CIPS films (**Section III**). **Section IV** summarizes the obtained results. **Supplementary Materials** elaborate on a mathematical formulation of the problem and the table of material parameters.

II. PROBLEM FORMULATION

Let us consider an epitaxial thin CIPS film sandwiched between the semiconducting electrodes with a screening length λ , which is clamped on a thick rigid substrate [see **Fig. 1(a)**]. Arrows show the out-of-plane ferroelectric polarization P_3 , directed along the X_3 -axis. The perfect electric contact between the film and the electrodes provides the effective screening of the out-of-plane polarization by the electrodes and precludes the domain formation for small enough λ . An electric voltage is applied between the electrodes. The misfit strain u_m originates from the film-substrate lattice constants mismatch and exists entire the film depth [15, 16, 17], because the film thickness h is regarded smaller than the critical thickness h_d of misfit dislocations appearance.

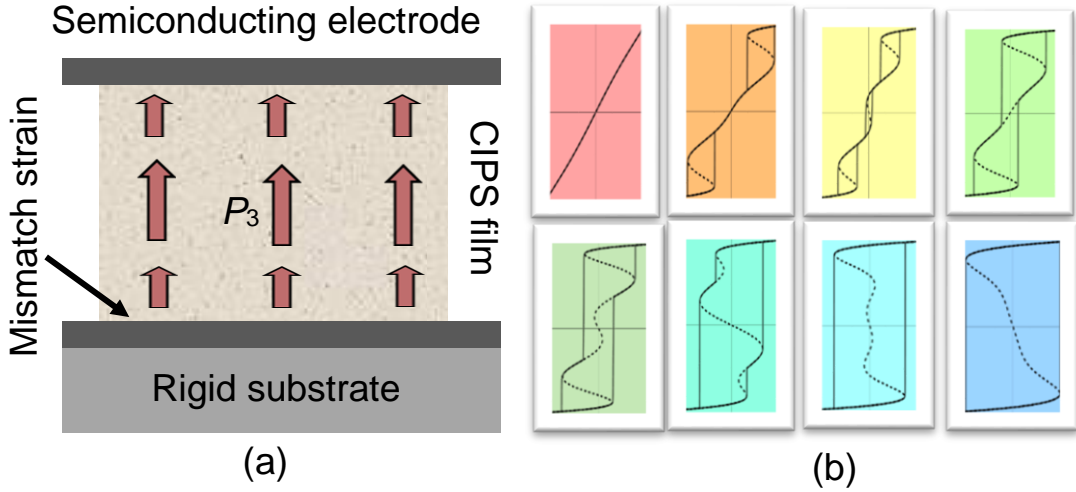


FIGURE 1. (a) Schematics of a thin epitaxial CIPS film sandwiched between semiconducting electrodes with a small screening length λ , and clamped on a rigid substrate. Arrows show the direction of the single-domain spontaneous polarization. (b) Schematics of the possible strain-induced changes of polarization reversal hysteresis loops. The part (a) is adapted from Ref. [10].

Within the LGD approach, the value and orientation of the spontaneous polarization P_i in thin ferroelectric films are controlled by the temperature T and mismatch strain u_m . For the validity of the continuum media approximation, the film thickness is regarded to be much bigger

than the lattice constant c . As a rule, the condition $c \ll h < h_d$ is valid for the film thickness range (5 – 50) nm.

It has been shown in Refs.[9 - 12] that the LGD free energy density of CIPS, g_{LGD} , has four potential wells at $\vec{E} = 0$. The density g_{LGD} includes the Landau-Devonshire expansion in even powers of the polarization P_3 (up to the eighth power), the Ginzburg gradient energy, the elastic and electrostriction energies. The behavior of polarization P_3 , piezoelectric coefficient d_{33} , and pyroelectric coefficient Π_3 in the electric field E_3 follows from the time-dependent LGD equations, which have the form [9 - 10]:

$$\Gamma \frac{\partial P_3}{\partial t} + [\alpha - 2\sigma_i(Q_{i3} + W_{ij3}\sigma_j)]P_3 + (\beta - 4Z_{i33}\sigma_i)P_3^3 + \gamma P_3^5 + \delta P_3^7 - g_{33kl} \frac{\partial^2 P_3}{\partial x_k \partial x_l} = E_3, \quad (1a)$$

$$\Gamma \frac{\partial d_{33}}{\partial t} + [\alpha - 2\sigma_i(Q_{i3} + W_{ij3}\sigma_j) + 3(\beta - 4Z_{i33}\sigma_i)P_3^2 + 5\gamma P_3^4 + 7\delta P_3^6]d_{33} - g_{33kl} \frac{\partial^2 d_{33}}{\partial x_k \partial x_l} = (2Q_{33} + 2W_{i33}\sigma_i)P_3 + 4Z_{333}P_3^3. \quad (1b)$$

$$\Gamma \frac{\partial \Pi_3}{\partial t} + [\alpha - 2\sigma_i(Q_{i3} + W_{ij3}\sigma_j) + 3(\beta - 4Z_{i33}\sigma_i)P_3^2 + 5\gamma P_3^4 + 7\delta P_3^6]\Pi_3 - g_{33kl} \frac{\partial^2 d_{33}}{\partial x_k \partial x_l} = \alpha_T P_3 + \beta_T P_3^3 + \gamma_T P_3^5. \quad (1c)$$

Here, Γ is the Khalatnikov kinetic coefficient [18]. The coefficient α depends linearly on the temperature T , $\alpha(T) = \alpha_T(T - T_C)$, where T_C is the Curie temperature of a bulk ferroelectric. The coefficients β , γ , and δ are temperature independent. The values σ_i denote diagonal components of a stress tensor in the Voigt notation, and the subscripts $i, j = 1 - 6$. The values Q_{i3} , Z_{i33} , and W_{ij3} denote the components of a linear and nonlinear electrostriction strain tensors in the Voigt notation, respectively [19, 20]. The values g_{33kl} are polarization gradient coefficients in the matrix notation and the subscripts $k, l = 1 - 3$. The boundary condition for P_3 at the film surfaces S is regarded “natural”, i.e., $g_{33kl}n_k \frac{\partial P_3}{\partial x_l} \Big|_S = 0$, where \vec{n} is the outer normal to the surface.

The values of T_C , α_T , β , γ , δ , Q_{i3} , W_{ij3} , and Z_{i33} have been derived in Ref.[21] from the fitting of temperature-dependent experimental data for the dielectric permittivity [22, 23], spontaneous polarization [24], and lattice constants [25] as a function of hydrostatic pressure. Elastic compliances s_{ij} were calculated from ultrasound velocity measurements [26, 27]. The CIPS parameters are listed in **Table SI** in **Appendix A**.

Modified Hooke’s law, relating elastic strains u_i and stresses σ_j , is obtained from the relation $u_i = -\partial g_{LGD} / \partial \sigma_i$:

$$u_i = s_{ij}\sigma_j + Q_{i3}P_3^2 + Z_{i33}P_3^4 + W_{ij3}\sigma_j P_3^2. \quad (2)$$

For the considered geometry of a CIPS film the following relations are valid for homogeneous stress and strain components: $\sigma_3 = \sigma_4 = \sigma_5 = \sigma_6 = 0$, $u_1 = u_2 = u_m$ and $u_4 = u_5 = u_6 = 0$.

The value E_3 in Eq.(1a) is an electric field component co-directed with the polarization P_3 . E_3 is a superposition of external (E_0) and depolarization (E_d) fields. In the considered case of a very high screening degree by the semiconducting electrodes with a small screening length $\lambda \leq 0.1$ nm, the solutions, corresponding to the almost constant P_3 , are energetically favorable and the domain formation is absent, because the corresponding depolarization field, $E_d = \frac{-P_3}{\epsilon_0(\epsilon_b+h/\lambda)}$, is very small for $h/\lambda \gg 1$. To analyze a quasi-static polarization reversal, we assume that the period, $2\pi/\omega$, of the sinusoidal external field E_0 is very small in comparison with the Landau-Khalatnikov relaxation time, $\tau = \Gamma/|\alpha|$.

The electrocaloric (**EC**) temperature change ΔT_{EC} , can be calculated from the expression [28]:

$$\Delta T_{EC} = -T \int_{E_1}^{E_2} \frac{1}{\rho_P C_P} \left(\frac{\partial P}{\partial T} \right)_E dE \cong T \int_{E_1}^{E_2} \frac{1}{\rho_P C_P} \Pi_3 dE, \quad (3)$$

where ρ_P is the volume density, T is the ambient temperature, and C_P is the CIPS specific heat.

For ferroics the specific heat depends on polarization (and so on external field) and can be modeled as following:

$$C_P = C_P^0 - T \frac{\partial^2 g}{\partial T^2}, \quad (4)$$

where C_P^0 is the polarization-independent part of specific heat and g is the density of the LGD free energy (A.2). According to experiment, the specific heat usually has a maximum in the first order ferroelectric phase transition point, which height is about (10 – 30) % of the C_P value near T_C (see e.g. [29]). The mass density and the polarization-independent part of the CIPS specific heat of are $\rho_P = 3.415 \cdot 10^3$ kg/m³ and $C_P^0 = 3.40 \cdot 10^2$ J/(kg K) [30, 31], respectively.

III RESULTS AND DISCUSSION

A. The size- and strain-induced transitions of the piezoelectric, electrocaloric and pyroelectric properties of CIPS films

The out-of-plane spontaneous polarization, P_s , piezoelectric coefficient, d_{33} , pyroelectric coefficient, Π_s , and electrocaloric temperature change, ΔT_{EC} , as a function of the film thickness h and misfit strain u_m , are shown in **Figs. 2, 3** and **4** for the temperatures $T = 250$ K, 293 K and 330 K, respectively. The abbreviations “PE”, “FE1” and “FE2” mean the paraelectric phase, high-polarization and low-polarization ferroelectric states, respectively.

The color maps of the spontaneous polarization, shown in **Figs. 2(a), 3(a)** and **4(a)**, are calculated by a conventional numerical minimization of the free energy (S.1) listed in **Appendix B**. The color scale in the maps shows the absolute value of P_s in $\mu\text{C}/\text{cm}^2$ calculated in the deepest

potential well of the LGD free energy. A sharp wedge-like region of the PE phase, which is stable at small thickness $h < 10$ nm and small strains $|u_m| < 1\%$, separates two ferrielectric states, FI1 and FI2, which correspond to big and small amplitudes of the out-of-plane spontaneous polarizations P_3^\pm , respectively. The area and height of the PE phase region significantly increases with the temperature increase, being the smallest for 250 K and the biggest for 330 K. The increase occurs because higher compressive or tensile strains are required to support the FI1 or FI2 polar states, respectively, when the growing temperature increases the coefficient $\alpha(T)$ in Eqs.(1). The unusual features of the color maps are the high-polarization FI1 state existing at compressive strains $u_m < 0$, and the low-polarization state FI2 existing for tensile strains $u_m > 0$. The FI1 and FI2 states either transform into one another for very small u_m or undergoes the first or second order phase transitions to the PE phase. The situation, shown in **Fig. 2** for $u_m > 0$, is anomalous for the most uniaxial and multiaxial ferroelectric films, where the out-of-plane polarization is absent or very small at $u_m > 0$, and the region of the FE c-phase vanishes or significantly constricts for $u_m > 0$ [15].

The color maps of the piezoelectric coefficient, d_{33} , shown in **Figs. 2(b), 3(b) and 4(b)**, are calculated using Eqs.(1a) and (1b) for $E_0 \rightarrow 0$. The color scale in the maps shows the absolute value of d_{33} in pm/V. Thin white curves in the plots correspond to the regions where d_{33} diverges at the boundary of the paraelectric-ferroelectric phase transition. The piezoelectric response is smaller in the FI1 state and higher in the FI2 state; and is absent inside the wedge-like region of the PE phase separating the FI states. Relatively small values of d_{33} in the high-polarization FI1 state are explained by the weak field dependence of the saturated out-of-plane spontaneous polarization. Note that d_{33} reaches (60 – 200) pm/V near the PE-FI2 boundary, being the smallest for 330 K and the biggest for 250 K.

The color maps of the pyroelectric coefficient, Π_s , shown in **Figs. 2(c), 3(c) and 4(c)**, are calculated using Eqs.(1a) and (1c) for $E_0 \rightarrow 0$. The color scale in the maps shows the absolute value of Π_s in mC/(K m²). Thin white curves in the plots correspond to the regions where Π_s diverges at the boundary of the paraelectric-ferroelectric phase transition. The pyroelectric response is smaller in the FI1 state and significantly higher in the FI2 state; and is absent in the PE phase. Higher values of Π_s in the low-polarization FI2 state are explained by the stronger field dependence of the unsaturated out-of-plane low-polarization. Despite the Π_s does not exceed 1 mC/(K m²) far from the paraelectric-ferroelectric boundary, the field behavior of Π_s determines the features of electrocaloric properties in accordance with Eq. (3).

The color maps of the electrocaloric temperature change, ΔT_{EC} , shown in **Figs. 2(d), 3(d) and 4(d)**, are calculated using Eqs.(1a), (1c) and (3)-(4) for $E_0 \rightarrow E_c$, where E_c is the coercive field

of the film. The color scale in the maps shows the value of ΔT_{EC} in K. The electrocaloric response is smaller in the FI2 state and significantly higher in the FI1 state; and is absent in the PE phase. Namely, ΔT_{EC} reaches minimum $\sim -(2 - 2.5)$ K near the PE-FI1 boundary for $-1\% < u_m < -0.5\%$ and $40 \text{ nm} < h < 10 \text{ nm}$. Higher negative values of ΔT_{EC} in the high-polarization FI1 state are related with the increase of the spontaneous polarization and with the features of the electrostriction coupling in CIPS, where the linear and nonlinear coefficients, Q_{i33} and Z_{i33} , linearly depend on temperature (see **Table SI** in **Appendix A**). Note that ΔT_{EC} cannot exceed -2.5 K for a bulk BaTiO₃ [28], which spontaneous polarization (about $25 \mu\text{C}/\text{cm}^2$ at room temperature) is much higher than the CIPS polarization (about $5 \mu\text{C}/\text{cm}^2$ at room temperature). The negative sign of the electrocaloric effect and its maximum predicted in compressed CIPS films, can be useful for the strain engineering of ultra-thin nano-coolers.

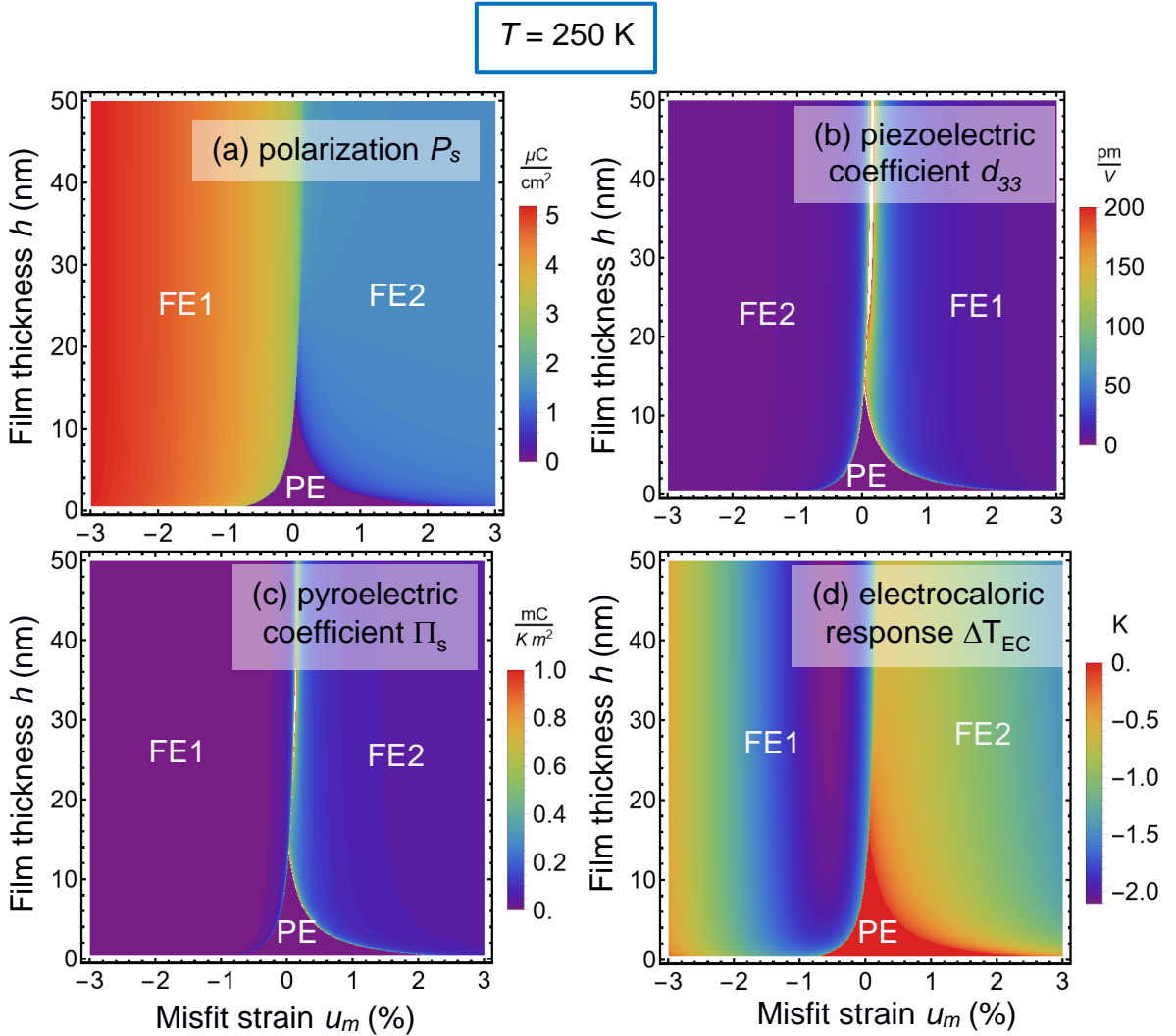


FIGURE 2. The spontaneous polarization P_s (a), piezoelectric coefficient d_{33} (b), pyroelectric coefficient Π_s (c), and the electrocaloric temperature change ΔT_{EC} (d) of a single-domain CIPS

film calculated as a function of the film thickness h and misfit strain u_m for $\lambda = 0.1$ nm and temperature $T = 250$ K. Color scales show the values of P_s , d_{33} , Π_s and ΔT_{EC} in $\mu\text{C}/\text{cm}^2$, pm/V , $\text{mC}/(\text{K m}^2)$, and K , respectively. White areas in the plots of d_{33} and Π_s correspond to the regions, where these values diverge. The abbreviations “PE”, “FE1” and “FE2” mean the paraelectric phase, high and low polarization ferrielectric states, respectively.

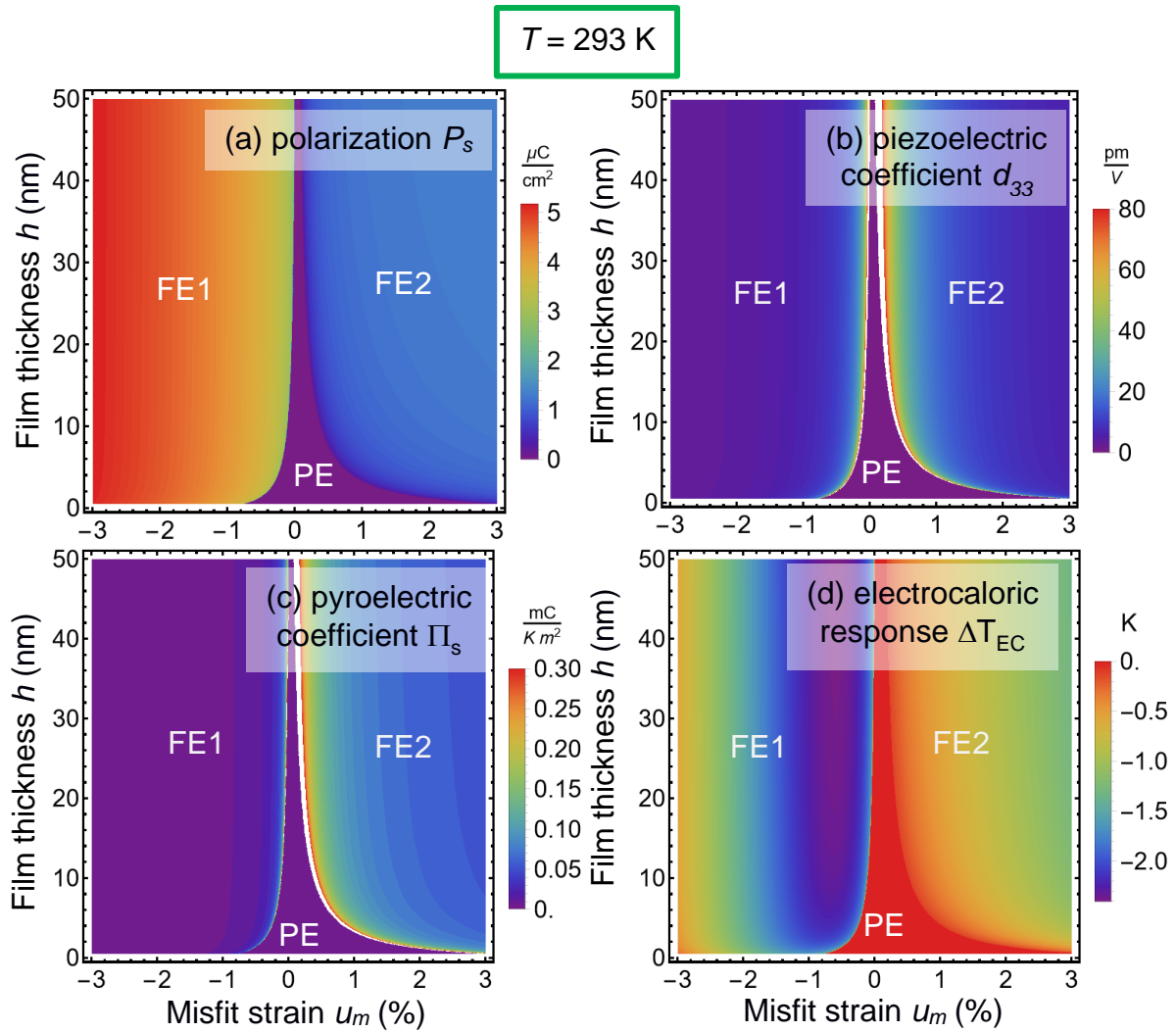


FIGURE 3. The spontaneous polarization P_s (a), piezoelectric coefficient d_{33} (b), pyroelectric coefficient Π_s (c), and the electrocaloric temperature change ΔT_{EC} (d) of a CIPS film calculated as a function of the film thickness h and misfit strain u_m for the room temperature $T = 293$ K. Other parameters and designations the same as in **Fig. 2**.

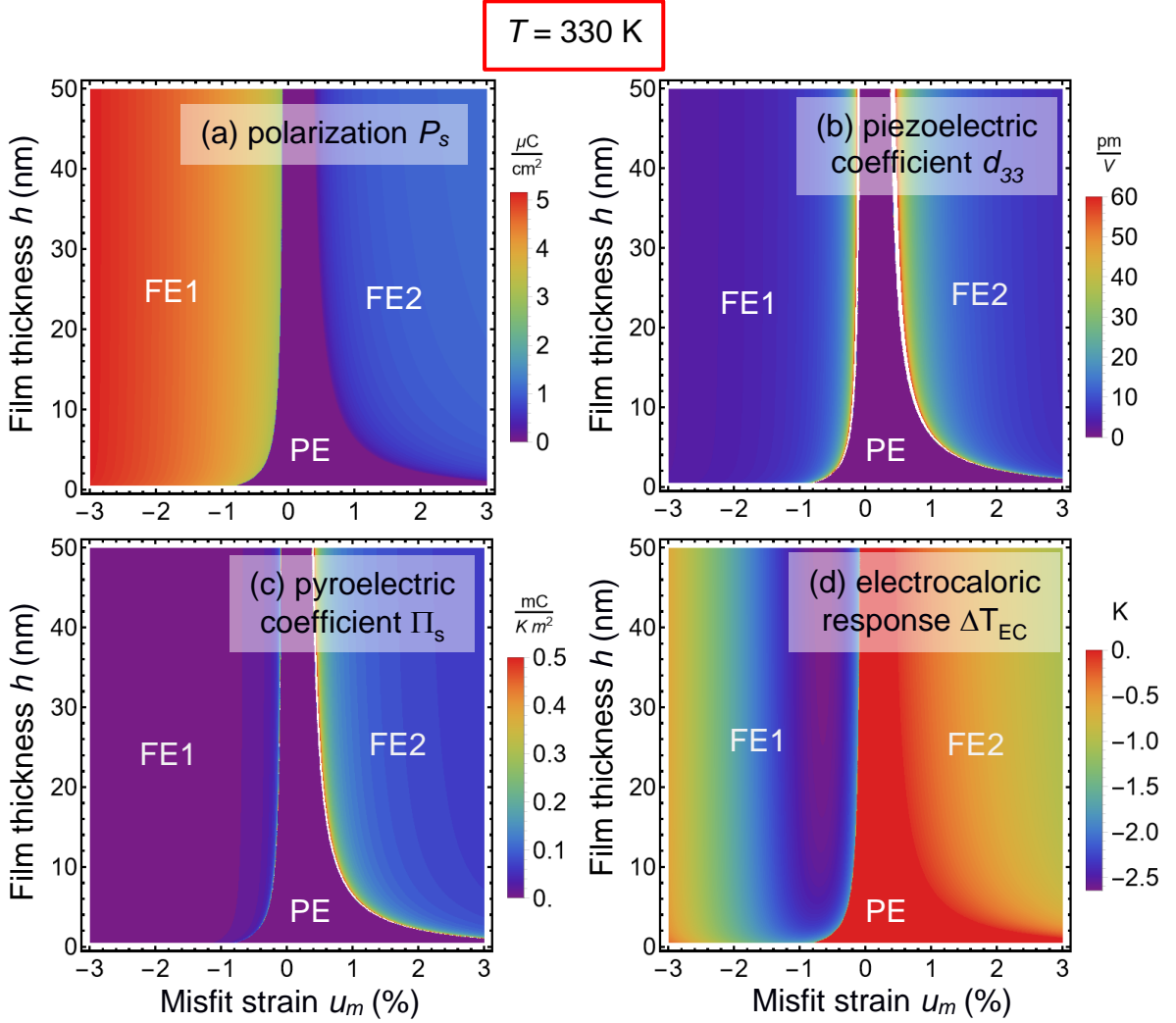


FIGURE 4. The spontaneous polarization P_s (a), piezoelectric coefficient d_{33} (b), pyroelectric coefficient Π_s (c), and the electrocaloric temperature change ΔT_{EC} (d) of a CIPS film calculated as a function of the film thickness h and misfit strain u_m for the temperature $T = 330 \text{ K}$. Other parameters and designations the same as in **Fig. 2**.

B. Polarization behavior in CIPS films on a patterned substrate

Let us consider a CIPS film placed on a patterned rigid substrate. Approximate analytical solutions for the CIPS polarization and related properties is possible if the average period of the patterns is much higher than the correlation length in the CIPS film. The assumption is true for smooth corrugations with a period more than 10 nm far from the temperature of CIPS phase transition. Let us illustrate the situation using a model 2D approximation for the normal and tangential strains induced by the patterns.

Typical profiles of vertical elastic displacement, $U(x)$, and tangential strain, $u_{tt}(x)$, created by smooth periodic patterns, are shown in **Fig. 5(a)**. Here the corrugation height h_c is not

more than 10 nm, and its characteristic period K_c is about 1 μm . Since $h_c \ll K_c$ and K_c is much higher than the characteristic length of polarization correlations, L_c , and the film surfaces are perfectly screened (by electrodes and/or surface charges), the polarization and strain gradients are very small, and the domain formation is improbable. Thus, one can use the analytical approach of Kvasov and Tagantsev [17] for calculations of the polarization components P_i in dependence on the temperature T and tangential strain u_{tt} , which influence is qualitatively similar to the influence of mismatch strain in thin films [17]. Using results [17] and making the Legendre transformation of G to the strain-polarization representation, $\tilde{G} = G + u\sigma$, the renormalized free energy density is [10]:

$$\tilde{g}_{LD+ES} = \frac{\alpha^*}{2} P_n^2 + \frac{\beta^*}{4} P_n^4 + \frac{\gamma^*}{6} P_n^6 + \frac{\delta^*}{8} P_n^8 - P_n E_n. \quad (5a)$$

The coefficients α^* , β^* , γ^* , and δ^* in Eq.(6) depend on the strain, u_m , in particular:

$$\alpha^* = \alpha + \alpha_1 u_{tt} + \alpha_2 u_{tt}^2, \quad \beta^* = \beta + \beta_1 + \beta_2 u_{tt}, \quad \gamma^* = \gamma + \gamma_1 + \gamma_2 u_{tt}, \quad \delta^* = \delta + \delta_1. \quad (5b)$$

The dependence of the coefficients α_1 , α_2 , β_1 , β_2 , γ_1 , γ_2 and δ_1 on the electrostriction constants Q_{ij} , W_{ijk} and Z_{ijk} , and elastic compliances s_{ij} is listed in **Appendix B**. E_n is the sum of applied and depolarization field. Since the domain formation is unlikely especially for smooth corrugation considered hereinafter, the depolarization field contribution absent in Eq.(5).

Minimization of the free energy (5) at $E_n = 0$ gives us the dependence of spontaneous polarization P_s on T and u_{tt} , which shown in **Fig. 5(b)**. The boundary between the PE phase and FI states, as well as their coexistence region, are superimposed on the polarization color maps. White dashed curves are the boundaries of the FI phase absolute instability. White dotted curves correspond to the condition $\alpha^* = 0$. Black dashed vertical lines show the condition $\beta^* = 0$. Empty black and white circles denote the critical end point (CEP) marked by a black circle, and the bicritical end point (BEP) marked by a white circle [9 - 10]. The diagram contains a relatively big region of the PE phase located at $T > 300$ K and tensile strains $u_{tt} > 0$. The rest of the diagram is filled by the FI phase, which has two ferrielectric states, FI1 and FI2, with big and small amplitudes of the out-of-plane spontaneous polarizations P_s^\pm . The FI1 state can coexist with the PE phase for tensile strains (see the FI1+PE region). The PE-FI2 boundary is the second order phase transition at tensile strains $u_{tt} > 0$, and PE-FI1 boundary is the first order transition at compressive strains $u_{tt} < 0$.

The unusual feature of the corrugated CIPS layer diagram is that the high-temperature FI1 state exists at compressive strains $u_{tt} < 0$. The FI1 state does not vanish for a tensile strain $u_{tt} > 0$; instead, it continuously transforms in the FI2 state which polarization becomes small at $u_{tt} > 0$ and eventually undergoes the second order phase transition to the PE phase at the dotted line.

The magnitude of P_s is big for $u_{tt} > 0$ and small for $u_{tt} < 0$. The situation for $u_{tt} > 0$ is untypical for the most uniaxial and multiaxial ferroelectric films, where the out-of-plane polarization is absent or very small at $u_{tt} > 0$, the region of FE c-phase vanishes or significantly constricts for $u_{tt} > 0$, and increases for $u_{tt} < 0$.

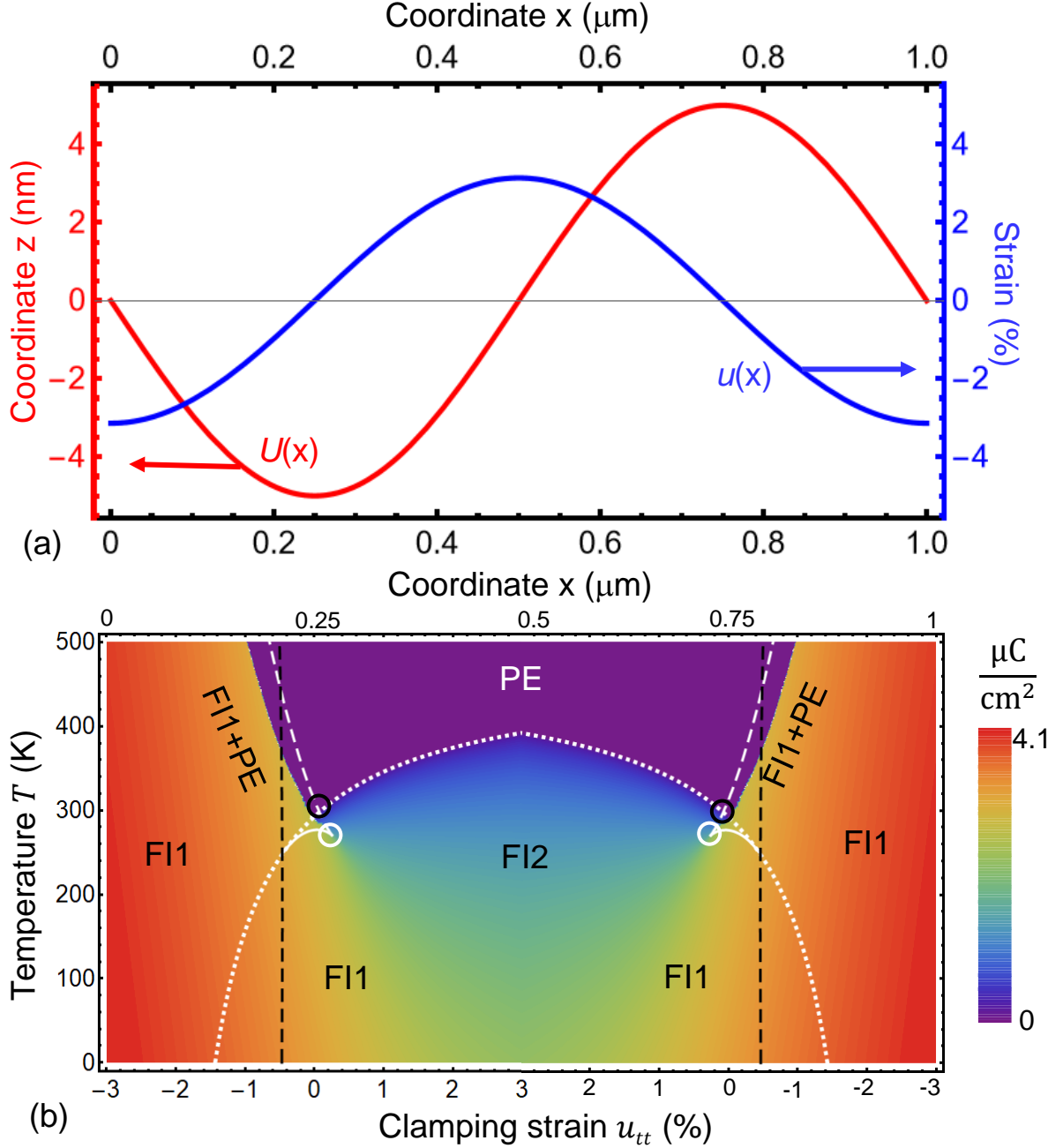


FIGURE 5. (a) Profiles of vertical elastic displacement, $U(x)$, and strain $u_{tt}(x)$ created by smooth periodic patterns. (b) The dependence of the spontaneous polarization P_s on temperature T and tangential strain u_{tt} . A color scale shows the polarization values in the deepest potential well of the LGD free energy. PE is the paraelectric phase, FI1 and FI2 are ferrielectric states 1 and 2; the CEP is marked by a white circle, and the BEP is marked by a black circle. The dotted and dashed curves, and circles are described in the text.

IV. SUMMARY

- We consider an epitaxial thin CIPS film sandwiched between semiconducting electrodes, and clamped on a thick rigid substrate, which create the mismatch strain in the film. Using LGD phenomenological approach, we study the piezoelectric, electrocaloric and pyroelectric properties of the strained film and reveal an unusually strong effect of a mismatch strain on these properties.
- We revealed that the sign of the mismatch strain and its magnitude determine the behavior of piezoelectric, electrocaloric and pyroelectric responses. In particular, the strain effect on these properties is opposite, i.e., “anomalous”, in comparison with many other ferroelectric films, for which the out-of-plane remanent polarization, piezoelectric, electrocaloric and pyroelectric increase strongly for tensile strains and decrease or vanish for compressive strains. The negative sign of the electrocaloric effect and its maximum predicted in compressed CIPS films, can be useful for the strain engineering of ultra-thin nano-coolers.
- The calculated phase diagram of the CIPS film on a patterned substrate demonstrates how the modulation of a tangential strain, created by the patterns, induces the transition between the two ferrielectric states with low and high polarization. Also, we studied the conditions when the piezoelectric, electrocaloric and pyroelectric responses can reach maximal values for small electric fields.

Acknowledgements. A.N.M. and A.L.K. acknowledge support from the Horizon Europe Framework Programme (HORIZON-TMA-MSCA-SE), project № 101131229, Piezoelectricity in 2D-materials: materials, modeling, and applications (PIEZO 2D). A.N.M., E.A.E. and L.P.Y. acknowledge support from the National Academy of Sciences of Ukraine. S.V.K. was supported by the center for 3D Ferroelectric Microelectronics (3DFeM), an Energy Frontier Research Center funded by the U.S. Department of Energy (DOE), Office of Science, Basic Energy Sciences under Award Number DE-SC0021118. This work (A.L.K.) was developed within the scope of project CICECO-Aveiro Institute of Materials (UIDB/50011/2020 & UIDP/50011/2020) financed by national funds through the FCT-Foundation for Science and Technology (Portugal).

Data availability statement. Numerical results presented in the work are obtained and visualized using a specialized software, Mathematica 13.2 [32]. The Mathematica notebook, which contain the codes, is available per reasonable request.

Authors' contribution. A.N.M. formulated the problem, performed analytical calculations, analyzed results, and wrote the manuscript draft. E.A.E. and L.P.Y. wrote the codes. V.V.L., A.L.K., S.V.K. and Y.M.V. worked on the results explanation and manuscript improvement.

Supplementary Materials

APPENDIX A. LGD parameters for a bulk ferroelectric CuInP_2S_6

Table SI. LGD parameters for a bulk ferroelectric CuInP_2S_6 at fixed stress. Adapted from Refs.[9 - 10]

Coefficient	Numerical value
ϵ_b	9
α_T ($\text{C}^{-2}\cdot\text{m J/K}$)	1.64067×10^7
T_C (K)	292.67
β ($\text{C}^{-4}\cdot\text{m}^5\text{J}$)	3.148×10^{12}
γ ($\text{C}^{-6}\cdot\text{m}^9\text{J}$)	-1.0776×10^{16}
δ ($\text{C}^{-8}\cdot\text{m}^{13}\text{J}$)	7.6318×10^{18}
Q_{i3} ($\text{C}^{-2}\cdot\text{m}^4$)	$Q_{13} = 1.70136 - 0.00363 T$ $Q_{23} = 1.13424 - 0.00242 T$ $Q_{33} = -5.622 + 0.0105 T$
Q_h ($\text{C}^{-2}\cdot\text{m}^4$)	$-2.785 + 0.00445 T$
Z_{i33} ($\text{C}^{-2}\cdot\text{m}^4$)	$Z_{133} = -2059.65 + 0.8 T$ $Z_{233} = -1211.26 + 0.45 T$ $Z_{333} = 1381.37 - 12 T$
s_{ij} (Pa^{-1})	$s_{11} = 1.510\times 10^{-11}$ $s_{12} = 0.183\times 10^{-11}$

APPENDIX B. Free energy with renormalized coefficients

Using results [17] and making the Legendre transformation of Eq.(1) to the strain-polarization representation, $\tilde{G} = G + u\sigma$, the renormalized free energy density is [10]:

$$\tilde{g}_{LD+ES} = \frac{\alpha^*}{2} P_3^2 + \frac{\beta^*}{4} P_3^4 + \frac{\gamma^*}{6} P_3^6 + \frac{\delta^*}{8} P_3^8 - P_3 E_3. \quad (\text{S.1})$$

The coefficients α^* , β^* , γ^* , and δ^* in Eq.(S.1) depend on the strain, u_m , and film thickness h as:

$$\frac{\alpha^*}{2} = \frac{\alpha}{2} + \frac{1}{\epsilon_0(\epsilon_b + h/\lambda)} + \frac{u_m(Q_{23}(s_{12} - s_{11}) + Q_{13}(s_{12} - s_{22}))}{s_{11}s_{22} - s_{12}^2} - u_m^2 \frac{(s_{12} - s_{22})^2 W_{113} + (s_{11} - s_{12})^2 W_{223}}{2(s_{12}^2 - s_{11}s_{22})^2}, \quad (\text{S.2a})$$

$$\frac{\beta^*}{4} = \frac{\beta}{4} + \frac{Q_{23}^2 s_{11} - 2Q_{13}Q_{23}s_{12} + Q_{13}^2 s_{22}}{2(s_{11}s_{22} - s_{12}^2)} + u_m \left\{ \frac{(s_{22} - s_{12})Z_{133} + (s_{11} - s_{12})Z_{233}}{s_{12}^2 - s_{11}s_{22}} + \frac{Q_{23}(s_{12}(s_{12} - s_{22})W_{113} + s_{11}(s_{11} - s_{12})W_{223}) + Q_{13}(s_{22}(-s_{12} + s_{22})W_{113} + s_{12}(-s_{11} + s_{12})W_{223})}{(s_{12}^2 - s_{11}s_{22})^2} \right\}, \quad (\text{S.2b})$$

$$\begin{aligned}
\frac{\gamma^*}{6} = & \frac{\gamma}{6} + \frac{(Q_{13}s_{22} - Q_{23}s_{12})Z_{133} + (Q_{23}s_{11} - Q_{13}s_{12})Z_{233}}{s_{11}s_{22} - s_{12}^2} - \\
& \frac{-2Q_{13}Q_{23}s_{12}(s_{22}W_{113} + s_{11}W_{223}) + Q_{23}^2(s_{12}^2W_{113} + s_{11}^2W_{223}) + Q_{13}^2(s_{22}^2W_{113} + s_{12}^2W_{223})}{2(s_{12}^2 - s_{11}s_{22})^2} + \\
u_m & \frac{s_{22}^2W_{113}Z_{133} + s_{11}^2W_{223}Z_{233} - s_{12}(s_{22}W_{113} + s_{11}W_{223})(Z_{133} + Z_{233}) + s_{12}^2(W_{223}Z_{133} + W_{113}Z_{233})}{(s_{12}^2 - s_{11}s_{22})^2}, \quad (S.2c)
\end{aligned}$$

$$\begin{aligned}
\frac{\delta^*}{8} = & \frac{\delta}{8} + \frac{s_{22}Z_{133}^2 - 2s_{12}Z_{133}Z_{233} + s_{11}Z_{233}^2}{2(s_{11}s_{22} - s_{12}^2)} + \\
& \frac{Q_{23}(s_{12}(s_{22}W_{113} + s_{11}W_{223})Z_{133} - s_{12}^2W_{113}Z_{233} - s_{11}^2W_{223}Z_{233})}{(s_{12}^2 - s_{11}s_{22})^2} + \\
& \frac{Q_{13}(-s_{22}^2W_{113}Z_{133} + s_{12}s_{22}W_{113}Z_{233} + s_{12}W_{223}(-s_{12}Z_{133} + s_{11}Z_{233}))}{(s_{12}^2 - s_{11}s_{22})^2}. \quad (S.2d)
\end{aligned}$$

Since W_{ijk} are small enough, we remain only linear terms in W_{ijk} in Eqs.(S.2), and omit all terms proportional to higher powers of the parameter.

References

-
- [1] Y. Liu, J. F. Scott, B. Dkhil. Direct and indirect measurements on electrocaloric effect: Recent developments and perspectives. *Appl. Phys. Rev.* **3**, 031102 (2016).
- [2] R. Kumar, S. Singh, Giant electrocaloric and energy storage performance of $[(K_{0.5}Na_{0.5})NbO_3](1-x) - [LiSbO_3]x$ nanocrystalline ceramics. *Sci Rep.* **8**, 3186 (2018).
- [3] Zhao, J. Z., L. C. Chen, B. Xu, B. B. Zheng, J. Fan, and H. Xu. "Strain-tunable out-of-plane polarization in two-dimensional materials. *Phys. Rev. B* **101**, 121407 (2020).
- [4] Ju. Banys, A. Dziaugys, K. E. Glukhov, A. N. Morozovska, N. V. Morozovsky, Yu. M. Vysochanskii. [Van der Waals Ferroelectrics: Properties and Device Applications of Phosphorous Chalcogenides](#) (John Wiley & Sons, Weinheim 2022) 400 pp. ISBN: 978-3-527-35034-6
- [5] Zhi-Zheng Sun, Wei Xun, Li Jiang, Jia-Lin Zhong, and Yin-Zhong Wu. Strain engineering to facilitate the occurrence of 2D ferroelectricity in $CuInP_2S_6$ monolayer. *Journal of Physics D: Applied Physics* **52**, 465302 (2019).
- [6] Y.M. Vysochanskii, V.A. Stephanovich, A.A. Molnar, V.B. Cajipe, and X. Bourdon, Raman spectroscopy study of the ferrielectric-paraelectric transition in layered $CuInP_2S_6$. *Phys. Rev. B*, **58**, 9119 (1998).
- [7] N. Sivadas, P. Doak, and P. Ganesh. Anharmonic stabilization of ferrielectricity in $CuInP_2Se_6$. *Phys. Rev. Research* **4**, 013094 (2022).
- [8] J.A. Brehm, S.M. Neumayer, L. Tao, O'Hara, A., M. Chyasnovich, M.A. Susner, M.A. McGuire, S.V. Kalinin, S. Jesse, P. Ganesh, and S. Pantelides. Tunable quadruple-well ferroelectric van der Waals crystals. *Nat. Mater.* **19**, 43 (2020).

-
- [⁹] A. N. Morozovska, E.A. Eliseev, M. E. Yeliseiev, Yu. M. Vysochanskii, and D. R. Evans. Stress-Induced Transformations of Polarization Switching in CuInP₂S₆ Nanoparticles. *Physical Review Applied* **19**, 054083 (2023), <https://link.aps.org/doi/10.1103/PhysRevApplied.19.054083>
- [¹⁰] A. N. Morozovska, E. A. Eliseev, A. Ghosh, M. E. Yeliseiev, Y. M. Vysochanskii, and S. V. Kalinin. Anomalous Polarization Reversal in Strained Thin Films of CuInP₂S₆, *Phys. Rev. B*, **108**, 054107 (2023) <https://link.aps.org/doi/10.1103/PhysRevB.108.054107>
- [¹¹] A. N. Morozovska, E. A. Eliseev, Y. Liu, K. P. Kelley, A. Ghosh, Y. Liu, J. Yao, N. V. Morozovsky, A. L. Kholkin, Y. M. Vysochanskii, and S. V. Kalinin. Bending-induced isostructural transitions in ultrathin layers of van der Waals ferroelectrics, <https://doi.org/10.48550/arXiv.2305.15247>
- [¹²] Y. Liu, A. N. Morozovska, A. Ghosh, K. P. Kelley, E. A. Eliseev, J. Yao, Y. Liu, and S. V. Kalinin, Disentangling stress and curvature effects in layered 2D ferroelectric CuInP₂S₆. <https://doi.org/10.48550/arXiv.2305.14309>
- [¹³] X. Bourdon, V. Maisonneuve, V.B. Cajipe, C. Payen, and J.E. Fischer. Copper sublattice ordering in layered CuMP₂Se₆ (M=In, Cr). *J. All. Comp.* **283**, 122 (1999).
- [¹⁴] V. Maisonneuve, V. B. Cajipe, A. Simon, R. Von Der Muhll, and J. Ravez. Ferrielectric ordering in lamellar CuInP₂S₆. *Phys. Rev. B* **56**, 10860 (1997).
- [¹⁵] N.A. Pertsev, A.G. Zembilgotov, A. K. Tagantsev, Effect of Mechanical Boundary Conditions on Phase Diagrams of Epitaxial Ferroelectric Thin Films, *Phys. Rev. Lett.* **80**, 1988 (1998).
- [¹⁶] C. Ederer, and N.A. Spaldin, Effect of epitaxial strain on the spontaneous polarization of thin film ferroelectrics, *Phys. Rev. Lett.* **95**, 257601 (2005).
- [¹⁷] A. Kvasov and A.K. Tagantsev. Role of high-order electromechanical coupling terms in thermodynamics of ferroelectric thin films. *Phys. Rev. B* **87**, 184101 (2013).
- [¹⁸] L. D. Landau, and I. M. Khalatnikov. On the anomalous absorption of sound near a second order phase transition point. In *Dokl. Akad. Nauk SSSR* **96**, 496 (1954).
- [¹⁹] Yu. M. Vysochanskii, M.M. Mayor, V. M. Rizak, V. Yu. Slivka, and M. M. Khoma. The tricritical Lifshitz point on the phase diagram of Sn₂P₂(Se_xS_{1-x})₆. *Soviet Journal of Experimental and Theoretical Physics* **95**, 1355 (1989).
- [²⁰] A. Kohutych, R. Yevych, S. Perechinskii, V. Samulionis, J. Banys, and Yu. Vysochanskii. Sound behavior near the Lifshitz point in proper ferroelectrics. *Phys. Rev. B* **82**, 054101 (2010).
- [²¹] A. N. Morozovska, E. A. Eliseev, S. V. Kalinin, Y. M. Vysochanskii, and Petro Maksymovych. Stress-Induced Phase Transitions in Nanoscale CuInP₂S₆. *Phys. Rev. B* **104**, 054102 (2021).
- [²²] P. Guranich, V.Shusta, E.Gerzanich , A.Slivka, I.Kuritsa, O.Gomonnai. "Influence of hydrostatic pressure on the dielectric properties of CuInP₂S₆ and CuInP₂Se₆ layered crystals." *Journal of Physics: Conference Series* **79**, 012009 (2007).
- [²³] A. V. Shusta, A. G. Slivka, V. M. Kedylich, P. P. Guranich, V. S. Shusta, E. I. Gerzanich, I. P. Prits, Effect of uniaxial pressure on dielectric properties of CuInP₂S₆ crystals. *Scientific Bulletin of Uzhhorod University. Physical series*, **28**, 44 (2010).

-
- [²⁴] A. Kohutych, V. Liubachko, V. Hryts, Yu. Shiposh, M. Kundria, M. Medulych, K. Glukhov, R. Yevych, and Yu. Vysochanskii. Phonon spectra and phase transitions in van der Waals ferroics $MM'P_2X_6$, *Molecular Crystals and Liquid Crystals* (2022).
<https://doi.org/10.1080/15421406.2022.2066787>
- [²⁵] M. A. Susner, M. Chyasnovichyus, A. A. Poretzky, Q. He, B. S. Conner, Y. Ren, D. A. Cullen et al. Cation–Eutectic Transition via Sublattice Melting in $CuInP_2S_6/In_{4/3}P_2S_6$ van der Waals Layered Crystals. *ACS nano*, **11**, 7060 (2017)
- [²⁶] J. Banys, J. Macutkevicius, V. Samulionis, A. Brilingas & Yu. Vysochanskii, Dielectric and ultrasonic investigation of phase transition in $CuInP_2S_6$ crystals. *Phase Transitions: A Multinational Journal* **77:4**, 345 (2004).
- [²⁷] V. Samulionis, J. Banys, Yu. Vysochanskii, and V. Cajipe. Elastic and electromechanical properties of new ferroelectric-semiconductor materials of $Sn_2P_2S_6$ family. *Ferroelectrics* **257:1**, 113 (2001).
- [²⁸] A. N. Morozovska, E. A. Eliseev, M. D. Glinchuk, H. V. Shevliakova, G. S. Svechnikov, M. V. Silibin, A. V. Syta, A. D. Yaremkevich, N. V. Morozovsky, and V. V. Shvartsman. Analytical description of the size effect on pyroelectric and electrocaloric properties of ferroelectric nanoparticles. *Phys.Rev. Materials* **3**, 104414 (2019). <https://link.aps.org/doi/10.1103/PhysRevMaterials.3.104414>
- [²⁹] F. Jona, and G. Shirane. *Ferroelectric Crystals*, International Series of Monographs on Solid State Physics. Pergamon press (1962).
- [³⁰] A. Inaba (2004) <http://www.chem.sci.osaka-u.ac.jp/lab/micro/report/rcmt/2004/2004res02>.
- [³¹] K. Moriya, N. Kariya, I. Pritz, Yu M. Vysochanskii, A. Inaba, T. Matsuo, The Heat Capacity of $CuInP_2Se_6$, a Layer-Structured Selenodiphosphate. *Ferroelectrics* **346**, 143 (2007).
<https://doi.org/10.1080/00150190601182402>
- [³²] <https://www.wolfram.com/mathematica>